



## Continuous Tuneable Droplet Ejection via Pulsed Surface Acoustic Wave Jetting

|                               |   |
|-------------------------------|---|
| Journal:                      | <i>Soft Matter</i>  |
| Manuscript ID                 | SM-ART-12-2017-002534.R1  |
| Article Type:                 | Paper   |
| Date Submitted by the Author: | 09-Mar-2018   |
| Complete List of Authors:     | Castro, Jasmine; RMIT University, Micro/Nanophysics Research Laboratory<br>Ramesan, Shwathy; RMIT University, Micro/Nanophysics Research Laboratory<br>Rezk, Amgad; RMIT University, Micro/Nanophysics Research Laboratory<br>Yeo, Leslie; RMIT University, Micro/Nanophysics Research Laboratory |
|                               |   |

Cite this: DOI: 10.1039/xxxxxxxxxx

# Continuous Tuneable Droplet Ejection via Pulsed Surface Acoustic Wave Jetting

Jasmine O. Castro,<sup>a</sup> Shwathy R. Ramesan,<sup>a</sup> Amgad R. Rezk,<sup>a</sup> and Leslie Y. Yeo<sup>a</sup>Received Date  
Accepted Date

DOI: 10.1039/xxxxxxxxxx

www.rsc.org/journalname

We report a miniaturised platform for continuous production of single or multiple liquid droplets with diameters between 60 and 500  $\mu\text{m}$  by interfacing a capillary-driven self-replenishing liquid feed with pulsed excitation of focussed surface acoustic waves (SAWs). The orifice-free operation circumvents the disadvantages of conventional jetting systems, which are often prone to clogging that eventuates in rapid degradation of the operational performance. Additionally, we show the possibility for flexibly tuning the ejected droplet size through the pulse width duration, thus avoiding the need for a separate device for every different droplet size required, as is the case for systems in which the droplet size is set by nozzles and orifices, as well as preceding ultrasonic jetting platforms where the droplet size is controlled by the operating frequency. Further, we demonstrate that cells can be jetted and hence printed onto substrates with control over the cell density within the droplets down to single cells. Given that the jetting does not lead to significant loss to the cell's viability or ability to proliferate, we envisage that this versatile jetting method can potentially be exploited with further development for cell encapsulation, dispensing and 3D bioprinting applications.

## 1 Introduction

In the last decade, significant advances in additive manufacturing techniques have progressed the development of three-dimensional (3D) printers to a level where they are now sufficiently low cost, compact and simple to use, especially by non-specialists, thereby ushering a revolution in the widespread adoption of these printers even for personal home use, much like those heralded by their 2D predecessors—the dot matrix, inkjet and laser printers—in decades past<sup>1</sup>. It is anticipated that 3D bioprinting will follow a similar, albeit more limited, adoption trajectory, potentially introducing a revolution in regenerative medicine, given the exciting possibility of assembling 3D structures—cell by cell, tissue layer by tissue layer—that mimic complex organs<sup>2</sup>.

The technology for 3D bioprinting has essentially drawn from that associated with conventional 3D and their predicate 2D printing platforms, namely, inkjet printing (based on thermal, piezoelectric and electrohydrodynamic droplet generation mechanisms)<sup>3</sup>, pressure-driven techniques<sup>4</sup>, laser-assisted bioprinting<sup>5,6</sup>, and stereolithography<sup>7</sup>. Each technique has its own merit, but nevertheless suffers from various drawbacks when attempting to extend the technology for printing biomaterials. Bubble and

thermal jets, which are cost-effective printing solutions that allow fast and efficient delivery, and micron-scale resolution<sup>2,8</sup>, operate at high temperatures between 200 to 300 °C. This not only results in the occasional random and nonuniform droplet<sup>9</sup>, but is also extremely damaging to biomolecules and cells—especially stem cells which are prone to heat shock with mere temperature rises of as little as a few degrees<sup>10</sup>; a unique blend of bio-inks are therefore often necessary to isolate them from such heating effects<sup>11</sup>. Transient pore formation, for example, was observed during thermal inkjet printing, which were reported to heal after several hours, though longer term effects on the viability and proliferation of the cells were not examined<sup>12</sup>.

Piezoelectric and ultrasonic jets, on the other hand, do not cause as much heating but are also known to inflict considerable damage due to transient cavitation and hydrodynamic stresses<sup>13</sup>. Pressure-based methods, known for their compatibility with a broad range of fluid properties<sup>2</sup>, too have poor cell viability, especially due to the large shear stresses that the cells are exposed to when subjected to high extrusion pressures and speeds<sup>14</sup>. Additionally, these methods suffer from low print speeds and resolution, and are severely limited by the necessity for critically timing the gelation duration and the need to match the material and liquid densities in order to preserve the shape of the printed material<sup>9</sup>.

Laser-assisted bioprinting methods, in which a laser shock pulse is employed to vapourise the cell solution housed in a rib-

<sup>a</sup> School of Engineering, RMIT University, Melbourne, VIC 3001, Australia. E-mail: leslie.yeo@rmit.edu.au

bon in order to expel the cells from the liquid, have better cell viabilities compared to these other methods and are compatible with a wide range of materials. These methods, however, have limited printing capability in the third dimension, require complex and expensive optically-absorbing receiving substrates, and are susceptible to metallic contamination<sup>2,15,16</sup>. On the other hand, stereolithography—which offers nozzle-free printing, for example, of light-sensitive hydrogel layers with micron-dimension resolution<sup>17</sup>, is not widely used for bioprinting because the requisite photopolymers are mainly non-biocompatible or biodegradable and the residual photocuring reagents produce toxic effects that can also denature DNA<sup>18</sup>.

With the exception of laser-assisted bioprinting and stereolithography, all of the aforementioned methods require a nozzle or orifice through which the droplets are generated. This necessity, which the print quality critically hinges upon, is problematic for a number of reasons. Besides imposing considerable shear stress on the cells during extrusion of the material through the nozzle or orifice, which leads to higher cell mortality rates, they are extremely prone to clogging, which quickly leads to performance variability and degradation. The droplet size is also inextricably linked to the nozzle or orifice dimension, which needs the print head to be swapped every time a different droplet size is required. To circumvent the use of orifices or nozzles, Demirci & Montesano proposed the use of surface acoustic waves (SAWs)—nanometer amplitude MHz order electromechanical waves—in place of conventional low frequency (Hz to kHz order) vibration to pulse droplets through orifices which are much larger in dimension than the droplets themselves<sup>19</sup>. Another advantage of these high frequency waves are that they have lower propensity to damage biological entities—as demonstrated by their ability to print a wide variety of cells, even at much higher powers towards nebulisation<sup>20</sup>.

The tight correlation between the size of the printed droplet with the SAW frequency—which, in turn, is governed by the liquid's physical properties, predominantly its density and viscosity, due to the existence of a viscous penetration depth of the acoustic wave in the liquid<sup>21</sup>—is still a practical limitation. Flexibility in tuning the droplet size, or adjusting it to that required when altering the working fluid with different physical properties, remains only possible by using a different frequency device; in other words, it is not possible to flexibly tune the droplet dimension on demand using the same device. Moreover, an upper limit also exists since the sharper attenuation with increasing frequency results in shorter jet lengths<sup>22</sup>. If this decreases below the breakup length associated with the Rayleigh-Plateau instability,<sup>23</sup> droplets can no longer be produced. In any case, only a theoretical correlation between the droplet size and SAW frequency was reported in Ref. 19—the ability to alter the droplet dimension in this manner was never proven experimentally.

With the motivation of demonstrating a base platform that can potentially be developed for cell dispensing and encapsulation, as well as 3D bioprinting, capability, we adopt a different approach to that in Ref. 19, thus circumventing some of the abovementioned issues associated with that method. We attempt this by building on the SAW jetting technique of Tan *et al.*<sup>24</sup>,

which only demonstrated the jetting of a *single sessile drop without size control*. In order to adapt the technique for potential printing applications, we allow for repetitive droplet ejection on-demand through a means of continuous resupply to the parent drop reservoir, as well as the possibility for droplet size adjustment in a single fixed frequency device, whilst maintaining a nozzle-free solution.

## 2 Experimental Method

The fundamental premise of jetting a single sessile droplet using focussed SAWs is illustrated in the schematic in Figure 1a. Two opposing SAWs are generated on a chipscale single crystal piezoelectric substrate (lithium niobate; LiNbO<sub>3</sub>) by applying a sinusoidal electric signal at the resonant frequency to both circular electrode-width-controlled single-phase unidirectional transducers (SPUDTs)<sup>24</sup>; the SAW wavelength and hence the resonant frequency is set by the gap and width of the finger electrode patterns that make up the SPUDT<sup>25</sup>. As the travelling focussed SAWs from both ends of the device propagate along its surface and come into contact with the sessile droplet above, they diffract into the liquid at the Rayleigh angle ( $\approx 23^\circ$  to the vertical axis for water) to generate both acoustic streaming in the droplet as well as an acoustic radiation force at the droplet interface (Figure 1a)<sup>26</sup>; the former, i.e., acoustic streaming, has been exploited for driving a host of microfluidic actuation and particle manipulation schemes such as droplet<sup>27–32</sup> and microchannel transport<sup>33–37</sup>, mixing and particle concentration<sup>38–40</sup>, and nebulisation<sup>20,41–44</sup>, whereas the latter, i.e., the acoustic radiation force, has primarily been employed for bubble, droplet and particle manipulation in microchannels<sup>45–61</sup>. Given that the opposing but symmetric SAW pair has a focal point beneath the droplet, the viscous normal stress arising as a consequence of the acoustic streaming generated in the droplet together with the acoustic radiation force is imparted at the interface predominantly at the pole of the droplet that then extends the droplet upward to form an elongated jet<sup>24</sup>. If this extension is beyond the Rayleigh-Plateau breakup length, the jet then pinches off to form single or multiple droplets depending on the relative contributions between the destabilising inertial stress localised within the droplet due to the input SAW energy and the restoring capillary stress which is governed by the surface tension of the liquid.

To extend this technique for on-demand continuous jetting of size-tunable droplets, we engineered the integrated platform shown in Figure 1c,d consisting of a 3D printed liquid reservoir and chip holder together with the piezoelectric chip, which comprises a 23 mm x 10 mm x 0.5 mm 128° Y–X LiNbO<sub>3</sub> substrate. Focussed SAWs are generated on the chip with SPUDTs with a frequency  $f$  of 30 MHz, which corresponds to a wavelength  $\lambda_{\text{SAW}} = c_{\text{SAW}}/f = 130 \mu\text{m}$  given a SAW phase velocity  $c_{\text{SAW}} = 3990 \text{ m/s}$  in the substrate. We note that the placement of the reservoir interface is outside of the SAW propagation pathway to avoid damping of the acoustic wave. The liquid delivery from the reservoir to form a parent sessile droplet on the chip is then facilitated either through a 150  $\mu\text{m}$  wide and 5 mm long hy-

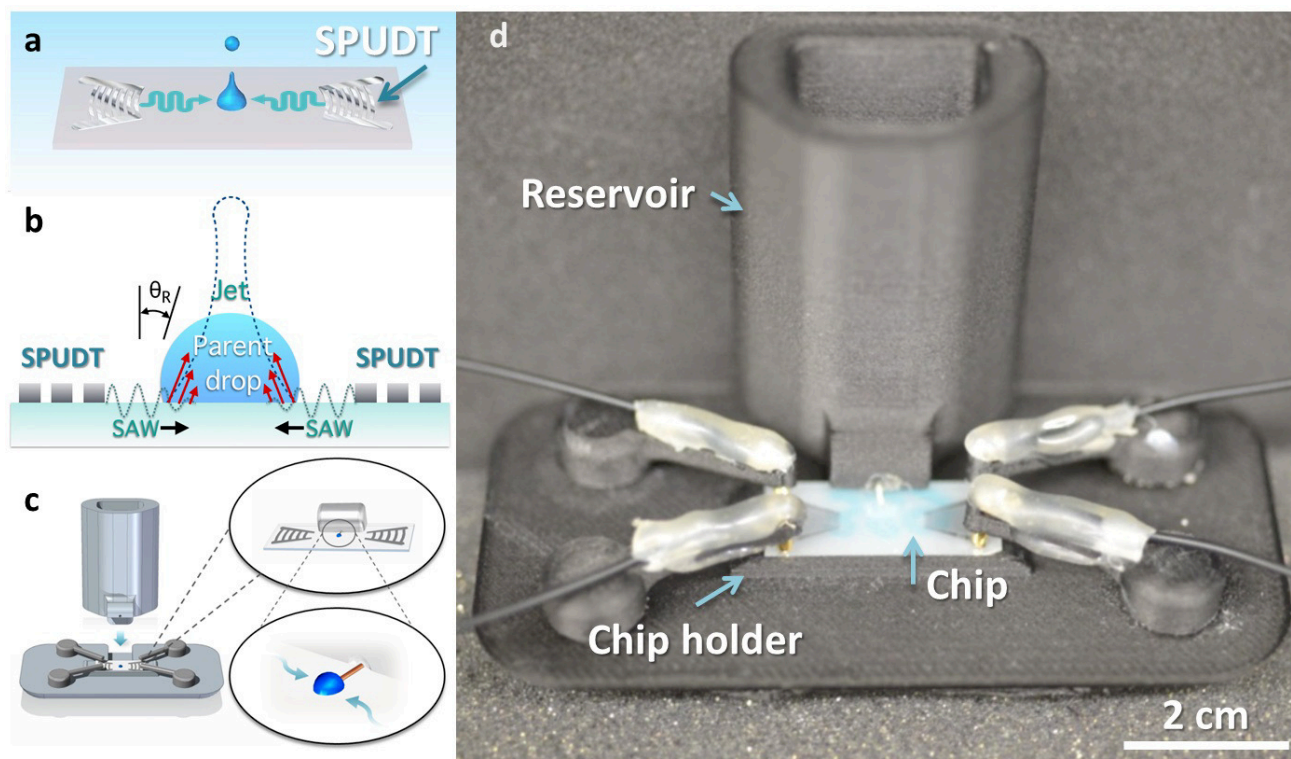


**Fig. 1** (a) Schematic illustration of the experimental setup (not to scale) used for the jetting of a *single* parent drop from a piezoelectric chip in Ref. 24. In that method, two opposing SAWs, generated by applying a sinusoidal electrical signal at resonance to the SPUDTs, are focussed beneath a sessile parent drop where they (b) leak their energy at the Rayleigh angle  $\theta_R$  into the drop to drive its elongation and jetting. (c) Schematic depiction (not to scale), and, (d) image of the experimental setup in the present work which integrates a liquid reservoir and self-feed together with the piezoelectric chip, housed in a chip holder. The insets show automatic refilling of the parent drop from the reservoir after each jetting event due to spontaneous capillary imbibition with the aid of a hydrophilic track that is formed by coating a thin hydrophobic silane layer around it or via a pulled capillary tube.

drophilic track confined within a hydrophobic barrier (given that LiNbO<sub>3</sub> is natively hydrophilic), or through a 150 μm inner diameter pulled capillary tube (PEEK Tubing; Labsmith Inc., Livermore, CA, USA). In either case, the track or tube is adjoined at the end by a 1 mm diameter circular hydrophilic region, above which the parent droplet sits, confined by the same hydrophobic barrier (see Figure 1c inset). This barrier is formed by spin-coating a thin (approximately 100 μm thick) layer of photoresist (SU-8 2010; Microchem Corp., Westborough, MA, USA)<sup>62</sup> followed by vapour deposition of an octadecyl(trichloro)silane<sup>63</sup> coating onto the substrate, thus providing a means by which liquid is imbibed from the reservoir, directly along the track or via the capillary tube, onto the circular region to form the parent drop.

Upon jetting this drop via application of a 30 MHz sinusoidal electrical pulse, generated using a signal generator (N9310A; Keysight Technologies Ltd., Mulgrave, VIC, Australia) and amplifier (ZHL-5W-1+; Mini-Circuits, Brooklyn, NY, USA), the liquid automatically refills due to spontaneous capillary action to form another sessile drop of the same diameter  $D_p$  that awaits the next jetting event. Control of this dimension, which, in turn, correlates with and hence allows tuning of the diameter of the ejected droplets  $D_j$ , as will be shown subsequently, is afforded through a balance of the replenishing flow under the hydrostatic pressure in the reservoir with the SAW pulse (and hence jetting) frequency.

Imaging of the parent drop deformation, jet development and droplet pinch-off was carried out using a high speed video camera (SA5, Photron Ltd, Tokyo, Japan) connected to a magnification lens (K2 Objective CF-4, Edmund Optics Inc., Barrington, NJ, USA) at frame rates between 7 and 30 kfps. The ejected droplets were measured by visual inspection of the acquired image frames: only those images immediately after which the ejected droplets returned to their spherical shape were considered in order to avoid shape distortion during the ejection event or their shrinkage due to droplet evaporation in-flight; the same droplet in three different frames was measured for statistical accuracy.

As a simple printing demonstration, we mounted the entire platform shown in Figure 1c,d onto a motorised  $x$ - $y$  translation stage (NRT100/M, Thorlabs Inc., Newton, NJ, USA), above which a Teflon<sup>®</sup>-coated glass slide (63434-02, Electron Microscopy Sciences, Hatfield, PA, USA) as the substrate to be printed on was placed; the vertical distance between the device and slide was approximately 0.3 cm. To briefly show the feasibility of the setup to potentially be extended for cell bioprinting applications, human embryonic kidney cells (HEK293; Sigma-Aldrich Pty. Ltd., Castle Hill, NSW, Australia) were suspended at known concentrations in Dulbecco's Modified Eagle Medium (GIBCO<sup>®</sup> DMEM) supplemented with 10% fetal bovine serum and 1% penicillin-streptomycin within the reservoir. The cells were subcultured periodically every 2–3 days and passaged at no more than 90% confluency. The incubator was constantly maintained at 37 °C with 95% relative humidity and 5% CO<sub>2</sub>. To verify the post-jetting cell viability, we conducted a trypan blue assay using the Neubauer chamber method<sup>64</sup>. The cell proliferation study, in which the post-jetting metabolic activity was assessed at 24 hour intervals over 72 hours, was carried out through an MTT (3-(4,5-dimethylthiazolyl-2)-2,5-diphenyltetrazolium bromide) as-

say<sup>65</sup>. The reduction of MTT by the metabolically active cells due to the dehydrogenase enzyme results in the formation of purple formazan crystals that are then imaged under brightfield illumination at 20X magnification (ZOE<sup>™</sup> Fluorescent Cell Imager, Bio-Rad Laboratories Inc., Hercules, CA, USA). After removal of the unreacted MTT solution from the wells, the crystals are solubilised by incubation in dimethyl sulfoxide (DMSO) over 30 min, and subsequently quantified via absorbance measurements of the solution at 570 nm (Spectramax<sup>®</sup> Paradigm multimode plate reader, Molecular Devices LLC, Sunnyvale, CA, USA). All cell culture media and supplements as well as the chemicals employed for the characterisation of the cells described above were acquired from Life Technologies Pty. Ltd. (Mulgrave, VIC, Australia), unless specified otherwise.

### 3 Results & Discussion

A phase map showing the different jetting regimes observed as a function of the power and SAW pulse width  $\Delta t$  (the duration over which the SAW is activated for each pulse) is shown in Figure 2a. It can be seen that a threshold power exists for the formation of a jet from the parent drop. Below this threshold, there is insufficient inertial energy to extrude a jet beyond a mere protrusion at its pole. In this case, the drop simply oscillates back and forth between its relaxed and elongated shape (regime i). Above this threshold power, three events are possible. For very short pulse widths, there is insufficient time for the jet to elongate, and the short energy burst results in its immediate breakup into a mist of very small droplets (regime ii). This bag breakup phenomenon is akin to the nebulisation process<sup>42</sup>. The critical pulse width—in this case, around 0.3 ms—corresponds to the characteristic jet breakup timescale, obtained by balancing the inertial and capillary stresses in the jet<sup>66</sup>:

$$\tau \sim \left[ \frac{\rho (D_j/2)^3}{\gamma} \right]^{1/2} \sim \mathcal{O}(10^{-1}) \text{ ms}; \quad (1)$$

$\rho$  and  $\gamma$  are the density and surface tension of the liquid, respectively. For pulse widths above this critical value, it can be seen that the jet elongates, forming a balloon at its tip due to the effect of strong capillary stresses acting there as a consequence of the end-cap curvature. The capillary stresses also subsequently cause the thread behind it to neck and pinch, thus ejecting a single droplet (regime iii). At higher powers, the longer extension of the thread leaves the jet susceptible to the classical Rayleigh-Plateau instability<sup>67,68</sup> in which varicose perturbations along its length are amplified exponentially with time when their wavelengths exceed the thread circumference, leading to its breakup to form multiple satellite droplets (regime iv).

The interplay between the inertial and capillary stresses, and its role in the different jetting behaviour observed in Figure 2a can be seen more clearly through a modified Weber number  $We$  (Figure 2a inset). Given that the inertia in the parent drop responsible for its deformation and potential elongation to extrude a jet originates from the mechanical energy transmitted into the drop by the SAW, and as this can be estimated by the input electrical

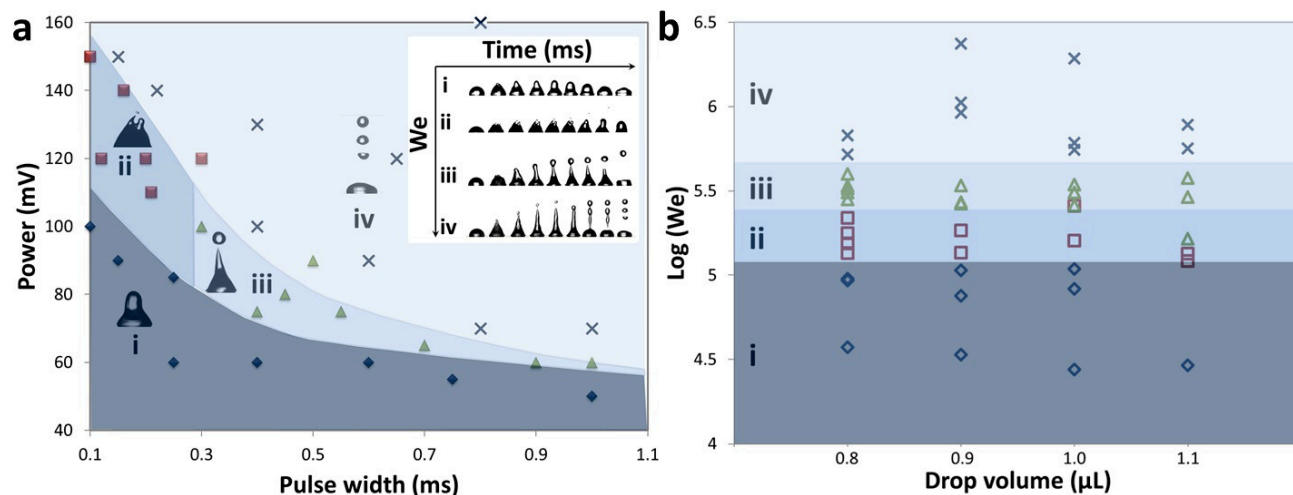


**Fig. 2** (a) Phase map showing the various jetting regimes obtained when an  $0.8 \mu\text{L}$  parent water drop is subject to a pulsed SAW with varying power and pulse width: (i) parent drop deformation, (ii) bag breakup, (iii) single droplet ejection, (iv) satellite droplet formation. The inset comprises image sequences showing the evolution of the parent drop for each regime as a function of the modified Weber number defined in Eq. (2) (regime i:  $0 < We < 10 \times 10^4$ ; regime ii:  $10 \times 10^4 < We < 26 \times 10^4$ ; regime iii:  $26 \times 10^4 < We < 40 \times 10^4$ ; regime iv:  $We > 40 \times 10^4$ ), which can be used to collapse the data in (b). Panel (b) also contains additional data beyond that in panel (a) for different parent drop volumes. The time between successive images in the inset in (a) is 5.0, 1.4, 3.4 and 4.0 ms, respectively, for each regime.

power to the device and the pulse width  $\Delta t$ , we define

$$We \equiv \frac{VI\Delta t}{\pi\gamma L}, \quad (2)$$

through which the data in Figure 2a can be collapsed, as shown in Figure 2b. In the above,  $V$  and  $I$  are the voltage and current of the input electrical signal applied to the SPUDT, and  $L$  is a characteristic deformation lengthscale of the parent drop.

Given that the tiny droplets produced by bag breakup in regime ii or the satellite droplet formation in regime iv typically lead to defects in the print quality, we now turn our attention to the single droplet ejection events in regime (iii), in particular, focussing on continuous jetting as well as the ability to vary the size of the ejected droplet without necessitating separate devices with different frequencies as that in Ref. 19. Both of these capabilities are demonstrated in Figure 3. Specifically, Figure 3a shows that the ejected droplet size can be tuned through the parent drop diameter, which, in turn, is controlled by the pulse frequency (number of pulses per second), as observed in Figure 3b. This is because shorter periods between pulses allow less time for replenishment of the liquid onto the device from the reservoir before the parent drop is jetted again and hence  $D_p$  concomitantly decreases. Through this simple adjustment of the pulse frequency from just 1 to 25 Hz, we were able to obtain a wide dynamic tuning range in the ejected droplet diameter between  $60 \mu\text{m}$  and  $500 \mu\text{m}$  on the same device. The possibility for continuous jetting is also captured in the data in Figure 3: each data point exhibits the average of three successive pulses (Figure 3a inset) at a specific pulse frequency that gives a particular parent drop diameter. It can thus be seen that the ejected droplet diameter is consistently maintained across successive pulses from the reasonably small upper and lower limits in the data, as depicted by the error bars.

To demonstrate the feasibility for the platform to potentially be used for bioprinting upon further development, we replaced the water feedstock solution in the reservoir with a suspension of HEK 293 cells in cell media and mounted the platform onto a motorised  $x$ - $y$  translation stage. Figure 4a-i shows a printed array of these droplets through successive pulsed SAW activation onto the Teflon<sup>®</sup>-coated glass slide mounted a short height above the device, in which relatively uniform printed droplet sizes and shapes were observed. We note the possibility of both printing upwards or downwards (Figure 4a-ii)—the latter by mounting the device upside down above the substrate—since the effect of gravity on the drops is negligible at these scales. Either configuration where the device is moved by mounting it on the translation stage over the stationary substrate, or, where the device is held in a fixed position with the substrate mounted on the translation stage and moved over the device, is possible.

As can be seen in Figure 4b, the number of cells in the ejected droplet that are thus printed can also be varied by adjusting either the cell concentration in the feedstock solution or the volume of the parent drop through the pulse frequency (Figure 3b). We not only observe the cell number within the ejected droplet to decrease both with the feedstock cell concentration and the size of the parent drop, but that it is also possible to achieve single cell ejection, which makes the platform particularly useful, for example, for sample dispensing into cell arrays for single cell analysis. On the other hand, the ability to tailor the number of cells that are printed is also useful in other applications, especially in tissue engineering or bioprinting where larger numbers of cells in a certain location are required. An application where the cell-laden droplets shown in Figure 4a-ii were inversely printed within a water-saturated incubator at  $37 \text{ }^\circ\text{C}$  for 24 hours would be particularly apt is in the generation of an array of 3D cell spheroids—

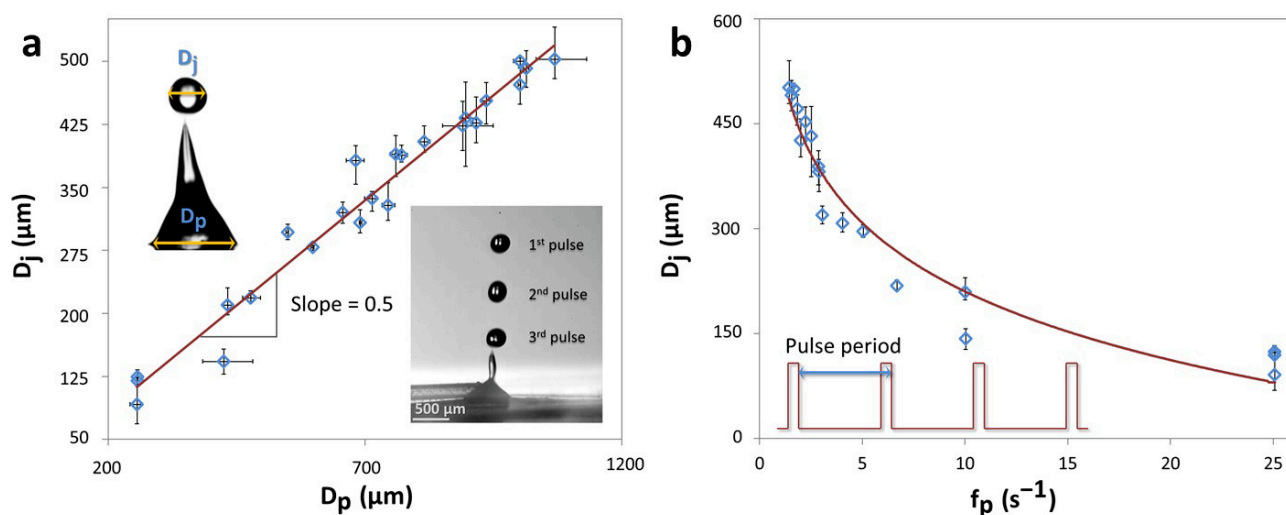


**Fig. 3** a) Correlation between the parent drop diameter  $D_p$  and the ejected droplet diameter  $D_j$ . Each data point comprises the upper and lower limits across measurements of the droplet diameter over triplicate continuous jetting experiments, each of which involving 3 ejected droplets from successive pulses, as shown in the image in the inset. (b) Relationship between  $D_j$  and the pulse frequency  $f_p$ . Unlike in (a), the trendline in (b) was added simply to facilitate ease of visualisation.

employed as realistic tumour mimics in drug testing—using the hanging droplet method<sup>69</sup>. As can be seen in the inset, the cells in the inversely printed pendant droplets quickly settle and aggregate at the bottom, which is the natural starting point for the culture of a single cell spheroid body. The cell printing technology presented here thus potentially represents a fast, user-friendly technique to automate the printing of uniform array clusters of these cell-laden hanging drops for large-scale spheroid culture. In addition, we also envisage the possibility of cell encapsulation for a plethora of drug delivery applications.

It is nevertheless crucial to verify that the cells are not adversely affected either by the acoustic radiation or heating during the jetting process. Using a trypan blue assay, we observe approximately 93% of the post-jetted cells to remain viable compared to the non-jetted control. Similarly, results of the MTT assay in Figure 4c show that the cells continue to proliferate normally over several days following jetting. These positive results are, nevertheless, not unexpected given that SAWs at much higher powers have been employed for nebulisation while maintaining decent viability<sup>20</sup>. A reason for this compared to the poorer cell fate obtained with other bioprinting techniques—in particular, piezoelectric printing methods—is the use of high MHz order frequencies in the current platform, which minimises the hydrodynamic stresses acting on the cell due to the rapid field reversal; moreover, unlike conventional piezoelectric jetting techniques which employ Hz to kHz order frequencies, the high frequencies ensure that cavitation, which is known to cause considerable structural and functional damage to cells, is not present.

## 4 Conclusion

A miniaturised jetting platform that can potentially be mounted on a print head, which does not require nozzles or orifices that are prone to clogging, and which does not result in appreciable loss in structural or functional viability of cells, would be attractive

for 3D bioprinting or cell encapsulation and dispensing applications. In an attempt to demonstrate its feasibility to potentially be developed for such applications, we show the possibility of exploiting a focussed SAW jetting device for continuous on-demand printing of size-controllable droplets. In particular, we interface a capillary-driven self-replenishing liquid delivery system with the SAW device and show that single, or multiple, droplets can be sequentially produced via pulsed excitation of the SAWs. The size of the droplets, across a range between 60  $\mu\text{m}$  and 500  $\mu\text{m}$ , were found to correlate closely to the parent drop size. This, in turn, can be controlled through the rate at which it is replenished through capillary refilling by adjusting the period between the pulses through the pulse frequency. This parameter, together with the cell concentration in the feedstock solution, was also found to facilitate tunability in the cell density within the droplets, down to single cell ejection. The cells were verified to remain highly viable and continued to proliferate normally after the jetting process.

## Conflicts of interest

There are no conflicts to declare.

## Acknowledgements

ARR is grateful for an RMIT University Vice-Chancellor's Post-doctoral Fellowship and LYY for an Australian Research Council (ARC) Future Fellowship (FT130100672). LYY also acknowledges funding from the ARC through Discovery Project (DP170101061).

## Notes and references

- 1 N. Jones, *Nature*, 2012, **487**, 22–23.
- 2 S. Murphy and A. Atala, *Nature Biotechnology*, 2014, **32**, 773–785.
- 3 T. Boland, T. Xu, B. Damon and X. Cui, *Biotechnology Journal*, 2006, **1**, 910–917.

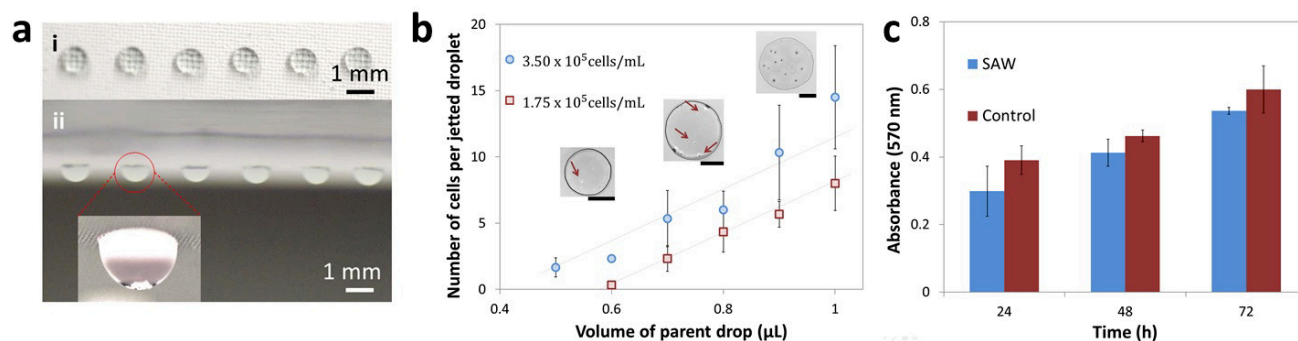
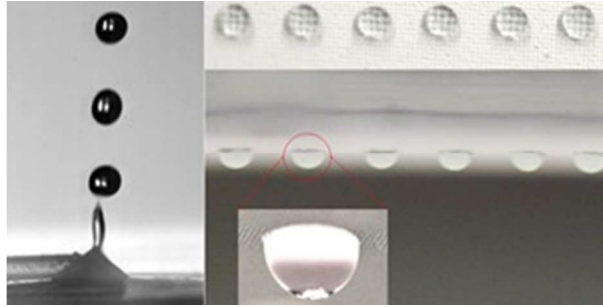


**Fig. 4** a) Linear array of uniform cell-laden (i) sessile and (ii) pendant droplets printed on a Teflon<sup>®</sup>-coated glass slide. The inset in (ii) shows cells sedimenting and aggregating at the bottom of the pendant droplet, typical of those in the hanging droplet method for 3D cell spheroid culture<sup>69</sup>. (b) Number of cells present in an ejected droplet as a function of the parent drop volume and the feedstock cell concentration. The slight departure from linearity at high cell concentrations suggests a practical limitation for the ‘bioink’ to be used with the platform, and the need to prevent the aggregation of cells in the feedstock solution. Trendlines were added to guide visualisation and the images above the data points provide a rough visual indication of the cell density in the ejected droplets that deposit on a collection slide; the scale bar below each image denoting a length of 500 μm. (c) Growth of post-jetted cells over 72 hours, quantified by the absorbance at 540 nm of dissolved formazan crystals converted from the MTT reagent by actively proliferating cells. The absorbance is directly proportional to the cell number in the solution. In (b) and (c), the error bars indicate the standard error of each set of experiments.

- 4 K. Iwami, T. Noda, K. Ishida, K. Morishima, M. Nakamura and N. Umeda, *Biofabrication*, 2010, **2**, 014108.
- 5 J. Barron, P. Wu, H. Ladouceur and B. Ringeisen, *Biomedical Microdevices*, 2004, **6**, 139–147.
- 6 F. Guillemot, A. Souquet, S. Catros, B. Guillotin, J. Lopez, M. Faucon, B. Pippenger, R. Bareille, M. Rémy, S. Bellance, P. Chabassier, J. Fricain and J. Amédec, *Acta Biomaterialia*, 2010, **6**, 2494–2500.
- 7 M. Ali, E. Pages, A. Ducom, A. Fontaine and F. Guillemot, *Biofabrication*, 2014, **6**, 045001.
- 8 J. Bharathan and Y. Yang, *Applied Physics Letters*, 1998, **72**, 2660–2662.
- 9 J. Li, M. Chen, X. Fan and H. Zhou, *Journal of Translational Medicine*, 2016, **14**, 271.
- 10 H. Omori, M. Otsu, A. Suzuki, T. Nakayama, K. Akama, M. Watanabe and N. Inoue, *Neuroscience Research*, 2014, **79C**, 13–21.
- 11 T. Xu, J. Jin, C. Gregory, J. Hickman and T. Boland, *Biomaterials*, 2005, **26**, 93–99.
- 12 X. Cui, D. Dean, Z. Ruggeri and T. Boland, *Biotechnology and Bioengineering*, 2010, **106**, 963–969.
- 13 R. Seetharam and S. Sharma, *Bioprocess Technology*, 1991, **12**, 3–315.
- 14 R. Chang, J. Nam and W. Sun, *Tissue Engineering, Part A*, 2008, **14**, 41–48.
- 15 B. Ringeisen, H. Kim, J. Barron, D. Krizman, D. Chrisey, S. Jackman, R. Auyeung and B. Spargo, *Tissue Engineering*, 2004, **10**, 483–491.
- 16 Y. Zhou, *Molecules*, 2016, **21**, 590.
- 17 Z. Wang, R. Abdulla, B. Parker, R. Samanipour, S. Ghosh and K. Kim, *Biofabrication*, 2015, **7**, 045009.
- 18 F. Melchels, J. Feijen and D. Grijpma, *Biomaterials*, 2010, **31**, 6121–6130.
- 19 U. Demirci and G. Montesano, *Lab on a Chip*, 2007, **7**, 1139–1145.
- 20 L. AlHasan, A. Qi, A. R. Rezk, L. Y. Yeo and P. Y. Chan, *Integrative Biology*, 2016, **8**, 12–20.
- 21 J. Friend and L. Yeo, *Reviews of Modern Physics*, 2011, **83**, 647–704.
- 22 M. Dentry, L. Yeo and J. Friend, *Physical Review E*, 2014, **89**, 013203.
- 23 J. Eggers, *Reviews of Modern Physics*, 1997, **69**, 865–929.
- 24 M. Tan, J. Friend and L. Yeo, *Physical Review Letters*, 2009, **103**, 024501.
- 25 R. Shilton, M. K. Tan, L. Y. Yeo and J. R. Friend, *Journal of Applied Physics*, 2008, **104**, 014910.
- 26 L. Y. Yeo and J. R. Friend, *Annual Review of Fluid Mechanics*, 2014, **46**, 379–406.
- 27 A. Wixforth, *Superlattices and Microstructures*, 2003, **33**, 389–396.
- 28 M. K. Tan, J. R. Friend and L. Y. Yeo, *Lab on a Chip*, 2007, **7**, 618.
- 29 M. Baudoin, P. Brunet, O. Bou Matar and E. Herth, *Applied Physics Letters*, 2012, **100**, 154102.
- 30 Y. Ai and B. L. Marrone, *Microfluidics and Nanofluidics*, 2012, **13**, 715–722.
- 31 A. Bussonnière, M. Baudoin, P. Brunet and O. B. Matar, *Physical Review E*, 2016, **93**, 053106–11.
- 32 J. T. Luo, N. R. Gerdali, J. H. Guan, G. McHale, G. G. Wells and Y. Q. Fu, *Physical Review Applied*, 2017, **7**, 014017–9.
- 33 M. K. Tan, L. Y. Yeo and J. R. Friend, *Europhysics Letters*, 2009, **87**, 47003.
- 34 L. Schmid, A. Wixforth, D. A. Weitz and T. Franke, *Microfluidics and Nanofluidics*, 2012, **12**, 229–235.
- 35 R. J. Shilton, M. Travagliati, F. Beltram and M. Cecchini, *Applied Physics Letters*, 2014, **105**, 074106.
- 36 M. B. Dentry, J. R. Friend and L. Y. Yeo, *Lab on a Chip*, 2014, **14**, 740–758.

- 37 A. Winkler, R. Brünig, C. Faust, R. Weser and H. Schmidt, *Sensors and Actuators A: Physical*, 2016, **247**, 259–268.
- 38 T. Frommelt, M. Kostur, M. Wenzel-Schäfer, P. Talkner, P. Hänggi and A. Wixforth, *Physical Review Letters*, 2008, **100**, 034502.
- 39 R. J. Shilton, L. Y. Yeo and J. R. Friend, *Sensors and Actuators B: Chemical*, 2011, **160**, 1565–1572.
- 40 G. Destgeer, J. H. Jung, J. Park, H. Ahmed and H. J. Sung, *Analytical Chemistry*, 2017, **89**, 736–744.
- 41 J. Ju, Y. Yamagata, H. Ohmori and T. Higuchi, *Sensors and Actuators A: Physical*, 2008, **145-146**, 437–441.
- 42 A. Qi, L. Y. Yeo and J. R. Friend, *Physics of Fluids*, 2008, **20**, 074103.
- 43 S. R. Heron, R. Wilson, S. A. Shaffer, D. R. Goodlett and J. M. Cooper, *Analytical Chemistry*, 2010, **82**, 3985–3989.
- 44 J. Ho, M. K. Tan, D. B. Go, L. Y. Yeo, J. R. Friend and H. C. Chang, *Analytical Chemistry*, 2011, **83**, 3260–3266.
- 45 T. Franke, A. R. Abate, D. A. Weitz and A. Wixforth, *Lab on a Chip*, 2009, **9**, 2625–2627.
- 46 S. S. Lin, X. Mao and T. J. Huang, *Lab on a Chip*, 2012, **12**, 2766–2770.
- 47 L. Schmid and T. Franke, *Lab on a Chip*, 2013, **13**, 1691–1694.
- 48 Y. Chen, S. Li, Y. Gu, P. Li, X. Ding, L. Wang, J. P. McCoy, S. J. Levine and T. J. Huang, *Lab on a Chip*, 2014, **14**, 924–930.
- 49 D. J. Collins, T. Alan and A. Neild, *Lab on a Chip*, 2014, **14**, 1595–1603.
- 50 J. Behrens, S. Langelier, A. R. Rezk, G. Lindner, L. Y. Yeo and J. R. Friend, *Lab on a Chip*, 2015, **15**, 43–46.
- 51 G. Destgeer, B. H. Ha, J. Park, J. H. Jung, A. Alazzam and H. J. Sung, *Analytical Chemistry*, 2015, **87**, 4627–4632.
- 52 L. Ren, Y. Chen, P. Li, Z. Mao, P. H. Huang, J. Rufo, F. Guo, L. Wang, J. P. McCoy, S. J. Levine and T. J. Huang, *Lab on a Chip*, 2015, **15**, 3870–3879.
- 53 F. Guo, Z. Mao, Y. Chen, Z. Xie, J. P. Lata, P. Li, L. Ren, J. Liu, J. Yang, M. Dao, S. Suresh and T. J. Huang, *Proceedings of the National Academy of Sciences of the United States of America*, 2016, **113**, 1522–1527.
- 54 K. Chen, M. Wu, F. Guo, P. Li, C. Y. Chan, Z. Mao, S. Li, L. Ren, R. Zhang and T. J. Huang, *Lab on a Chip*, 2016, **16**, 2636–2643.
- 55 W. Zhou, L. Niu, F. Cai, F. Li, C. Wang, X. Huang, J. Wang, J. Wu, L. Meng and H. Zheng, *Biomechanics*, 2016, **10**, 034121.
- 56 M. Sesen, C. Devendran, S. Malikides, T. Alan and A. Neild, *Lab on a Chip*, 2017, **17**, 438–447.
- 57 Z. Ma, Y. Zhou, D. J. Collins and Y. Ai, *Lab on a Chip*, 2017, **17**, 3176–3185.
- 58 M. Wu, Z. Mao, K. Chen, H. Bachman, Y. Chen, J. Rufo, L. Ren, P. Li, L. Wang and T. Huang, *Advanced Functional Materials*, 2017, **27**, 1606039.
- 59 Z. Mao, P. Li, M. Wu, H. Bachman, N. Mesyngier, X. Guo, S. Liu, F. Costanzo and T. Huang, *ACS Nano*, 2017, **11**, 603–612.
- 60 J. Park, J. Jung, G. Destgeer, H. Ahmed, K. Park and H. Sung, *Lab on a Chip*, 2017, **17**, 1031–1040.
- 61 J. Park, J. Jung, K. Park, G. Destgeer, H. Ahmed, R. Ahmad and H. Sung, *Lab on a Chip*, 2018, **18**, 422–432.
- 62 N. Shirtcliffe, S. Aqil, C. Evans, G. McHale, M. Newton, C. Perry and P. Roach, *Journal of Micromechanics and Micro-engineering*, 2004, **14**, 1384–1389.
- 63 N. Glass, R. Tjeung, P. Chan, L. Yeo and J. Friend, *Biomechanics*, 2011, **5**, 036501.
- 64 K. Louis and A. Siegel, in *Mammalian cell viability: methods and protocols*, ed. M. Stoddart, Springer, New York, 2011.
- 65 T. Mosmann, *Journal of Immunological Methods*, 1983, **65**, 55–63.
- 66 J. Eggers and E. Villermaux, *Reports on Progress in Physics*, 2008, **71**, 036601.
- 67 J. A. Plateau, *Statique expérimentale et théorique des liquides soumis aux seules forces moléculaires*, Gauthier-Villars, Ghent, 1873.
- 68 Lord Rayleigh, *Proceedings of the London Mathematical Society*, 1878, **10**, 4–13.
- 69 J. M. Kelm, N. E. Timmins, C. J. Brown, M. Fussenegger and L. K. Nielsen, *Biotechnology and Bioengineering*, 2003, **83**, 173–180.



79x39mm (96 x 96 DPI)

A versatile acoustic chipscale platform that can potentially be mounted as a printhead for cell encapsulation, dispensing and 3D bioprinting.